Songklanakarin J. Sci. Technol.
44 (5), 1238–1247, Sep. – Oct. 2022

http://www.sjst.psu.ac.th

Original Article

Multi-body bond graph modeling and simulation of a bio-inspired gust mitigating flapping wing UAV

S. H. Abbasi*, A. Mahmood, and Abdul Khaliq

Department of Electrical and Computer Engineering,
Sir Syed CASE Institute of Technology, Islamabad, 54000 Pakistan

Received: 12 May 2022; Revised: 22 June 2022; Accepted: 27 July 2022

Abstract

The small size of Unmanned Aerial Vehicles (UAVs) incurs many challenges, including concerns of flight stability during turbulence. To address this issue, birds as their natural counterparts have been studied in depth. This paper presents a biologically inspired Gust Mitigation System (GMS) for a flapping wing UAV (FUAV), inspired by the covert feathers of birds. The GMS uses electromechanical (EM) covert feathers that sense the incoming gust and mitigate it through deflection of these feathers. A multibody dynamic model of gust mitigating FUAV is developed by appending models of the subsystems including rigid body, propulsion system, flapping mechanism, and GMS installed to the wings, by using a bond graph modeling approach. The dynamic wing flexibility is modeled with a Euler-Bernoulli beam for realism. The simulation results show that wing flexibility enhances aerodynamic efficiency, and moreover, the performance of the proposed GMS for flexible wings is better than that of rigid wings during gusty airflows. A good agreement between experimental results with these simulations validates the proposed design as well as accuracy of the developed model.

Keywords: flapping wing uav, turbulence, bio-inspiration, gust mitigation system, bond graph modeling, simulation

1. Introduction

UAVs generally fly in the atmospheric boundary layer (ABL) that extends from the ground up to 400-1000m elevation, and is considered highly turbulent. Significant degradation in the performance of UAVs has been observed in the presence of strong gusts and intense turbulence. Furthermore, the most prominent reason of UAV loss at low altitude operations is adverse winds. Therefore, to enable stable UAV operation in turbulent conditions, a GMS is inevitable for optimal aircraft stability that decreases the risk of crashing down (Mohamed, Massey, Watkins, & Clothier, 2014).

Autopilot modules have reduced pilot workload and improved safety while operating in gusty weather. Each subsystem is interlinked with the UAV's central flight computer and empowers the flight crew to closely assess the desired flight path. Preemptive actions can be taken prior to facing bad weather and turbulent airflow, to reduce gusting intensity (Tian, Chao, Rhudy, Gross, & Wu, 2021). Ratti, Moon, and Vachtsevanos (2011) presented advanced avionics for UAVs that can achieve stabilization performance similar to that of large sized aircrafts. A Micro Architecture and Control (MARC) avionics design was developed considerably addressing weight limitations and power consumption of UAVs.

Mohamed *et al*. (2014) indicates that the current conventional reactive attitude sensors lack the necessary response times for attitude control in high turbulence environments. Therefore, they presented in great detail novel and emerging biologically inspired sensors, which can sense the disturbances before a perturbation is induced.

Blower and Wickenheiser (2011) have replicated the concept of avian primary feathers splaying mechanism in fixed wing UAVs and explored their use for turbulence mitigation. The design showed significant improvement in stability characteristics of UAVs; however, their usage for FUAVs has not been discussed and leaves an open gap for research.

*Corresponding author
Email address: abbasi882@gmail.com

All of the studies cited above were either for conventional aircrafts or for fixed wing UAVs. Therefore, to address the issue of gusts in the context of FUAVs, detailed study of birds was carried out and it revealed the interesting fact that during high turbulence airflows and gusty winds, birds take on intermittent flight, i.e., include non-flapping phase. The covert feathers during these intermittent gliding flights get activated to alleviate gusts (Abbasi & Mahmood, 2019a).

This research presents a novel distributed GMS for FUAV inspired by the biological covert feathers of birds. GMS comprises EM covert feathers integrated in flapping wings of UAV. GMS activates only at the time of turbulent airflows to mitigate gusts, while at all other times it remains tightly attached to the wing to retain the overall airfoil profile. It provides various flight advantages, including better maneuverability and enhanced stability during adverse wind environments.

The development and effectiveness of the GMS was investigated by the authors in (Abbasi & Mahmood, 2019a; Abbasi & Mahmood, 2019b) by incorporating it in a rigid wing and performing simulations. In order to ascertain the utility of proposed GMS for complete flexible FUAV, this study incorporates substantial enhancements summarized as follows. First, we present a comprehensive model of a complete FUAV comprising the main body and its allied accessories. These accessories include flapping mechanism, wings, and the propulsion system which comprises battery, motor, and the gear box. Second, wing flexibility is incorporated by modeling the FUAV wings as Euler-Bernoulli beams and its effects on gust mitigation and overall aerodynamic efficiency of the FUAV is described. Thirdly, GMS is incorporated in the model of flexible FUAV and a complete multi-body model of Gust mitigating flexible FUAV is presented. We utilize bond graph modeling (BGM) for developing the complete model and for performing simulations of Gust mitigating FUAV. Furthermore, we generate state space equations for in-depth analysis of internal dynamics. In the end, accuracy and efficacy of the proposed gust mitigating flexible FUAV are analyzed and compared with published experimental studies.

The overall structure of the article is as follows. In Section 2, the architecture of gust mitigating FUAV is presented. Section 3 covers bond graph model (BGM) formation of FUAV sub-systems leading to the making of a multibody model of complete gust mitigating flexible FUAV and an in-depth study of wing flexibility. To validate the accuracy of proposed design and to check its correctness, comparison of results with experimental studies and further discussion are given in Section 4. The final section includes conclusions and future work.

2. Bio-inspired FUAV Design

The Festo's Smart Bird (Send, 1992) is the FUAV under study in this research as a prototype. The technical data of the Festo's bird are as follows:

- Torso Length - 1.07 m
- Wing Span - 2.2 m
- Chord Length - 0.28 m
- Weight - 450gm
- Battery - 7.4 V, 450 mA
- Power requirement - 23 Watts
- Structure - Lightweight carbon fiber structure

A dynamic model of the system under investigation can be developed considering that the FUAV is composed of subsystems, namely the main body, motors, the flapping mechanism, rigid wings and GMS. The proposed GMS consist of 16 biomimetic EM covert feathers. Eight are incorporated in the wing's top surface and eight on wing's bottom surface. Single EM covert feather comprises flap, hinge, mechanical linkage, spring, piezoelectric transducer (PZT), controller, and the voice coil actuator. The FUAV wing is composed of a skeletal structure equipped with ribs and spars to carry loads. The design of GMS ensures that the wings retain their overall airfoil shape throughout flapping phases, as the EM covert feathers remain firmly attached to wings. At a time of high turbulence FUAV resorts to intermittent flight and GMS activates, rotating the EM feathers to allow strong gusts to transpire through the airframe with little impedance.

The flap rotates as a response to incident gust and gives signal to PZT that is acting as a sensor through mechanical linkage and spring. After receiving gust signal the PZT now acts as an actuator and produces an output signal dependent on the gust experienced and gives it to controller, which in turn generates desired control output. This control output (a current) is forwarded to the voice coil actuator, which moves out the shaft inside it and applies force on the flap that deflects out of wing. Consequently, the gust flows through the EM covert feathers with only minimal interaction with the wing's cross-sectional area.

3. Multibody Modeling

Modeling and simulation is a process by which we get information about how a model will respond without physically experimenting with it. Mathematical model generally represents the system in the form of equations. Bond graph modeling is a potent tool for modeling engineering systems, particularly when diverse physical domains are present. Additionally, bond graph sub-models can be reused smartly, since the bond graph models are non-causal (Karimian & Jahanbin, 2019). The proposed design is multi-domain, which is why the bond graph modeling approach is used in this study.

3.1 20-SIM software

The 20-SIM software was used in this research for bond graph modeling and simulation. The modeling software is very easy to use and generates the required details of the system including graphical interface and the system's equations. Subsequently, state space analysis is run including pole-zero plots, Nyquist plots, and Bode plots of the system (Karimian & Jahanbin, 2019).

3.2 Model of the main body

The FUAV's main body is taken as 6 DOF rigid body, which can perform both rotational and translational motions. The motion of a rigid body in space follows the equations below, based on Newton's second law of motion (Jahanbin, Ghafari, Ebrahimi, & Meghdari, 2016):

$$\dot{p}_x = F_x + m\omega_z \frac{P_y}{m} - m\omega_y \frac{P_z}{m} \qquad (3)$$

$$\dot{p}_y = F_y + m\omega_x \frac{P_z}{m} - m\omega_z \frac{P_x}{m} \tag{4}$$

$$\dot{p}_z = F_z + m\omega_y \frac{P_x}{m} - m\omega_x \frac{P_y}{m} \tag{5}$$

$$\dot{p}_{Jx} = \tau_x + J_y\omega_y \frac{PJ_z}{J_z} - J_z\omega_z \frac{PJ_y}{J_y} \tag{6}$$

$$\dot{p}_{Jy} = \tau_y + J_z\omega_z \frac{PJ_x}{J_x} - J_x\omega_x \frac{PJ_z}{J_z} \tag{7}$$

$$\dot{p}_{Jz} = \tau_z + J_x\omega_x \frac{PJ_y}{J_y} - J_y\omega_y \frac{PJ_x}{J_x} \tag{8}$$

Figure 1 shows the final BGM of the main body with a general motion in three-dimensional space. The state variables comprise the generalized momenta p_x, p_y, p_z, p_{jx}, p_{jy}, and p_{jz} at every inertia element. Six state-space equations are obtained from the above mentioned BGM because the number of energy storing elements is 6.

3.3 Model of the DC motors

A schematic diagram of the propulsion system of the flexible FUAV is given in Figure 2. The DC motors are powered by a battery and change electrical energy into mechanical energy. They comprise an electromechanical coupling and the armature, which further consists of inductance and resistance elements. The back EMF of the motors is presented as a gyrator in the BGM (Jahanbin *et al.*, 2016). The BGM of the DC motor is developed using the description above, and is presented Figure 3.

3.4 Model of the flapping mechanism

The slider crank used in flapping mechanism comprises two rods linked together and an arm, which is hinged at 90º angle to the rotating shaft. Input to the crank rod i-e velocity is applied as a source of flow. The corresponding BGM is shown in Figure 4. 1-junction ($1\dot{\theta}$) is used for depicting the motion of the crank. The inertia of the crank about its axis is shown as *I* element and the linear velocity of the connecting rod as ($1\dot{x}, 1\dot{y}$), whereas *I* elements show the mass of connecting rod. 1-junction($1\dot{\alpha}$) and modulated transformers (MTF) are used for rotational motion of the link (Jahanbin *et al.*, 2016).

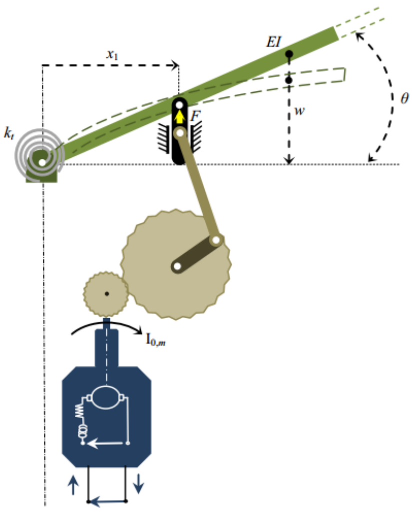

Figure 2. Schematic of the FUAV's propulsion system (Jahanbin *et al.*, 2016)

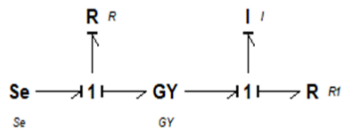

Figure 3. BGM of a DC motor

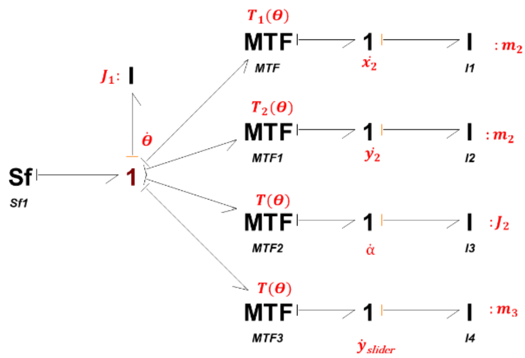

Figure 4. BGM of a flapping mechanism

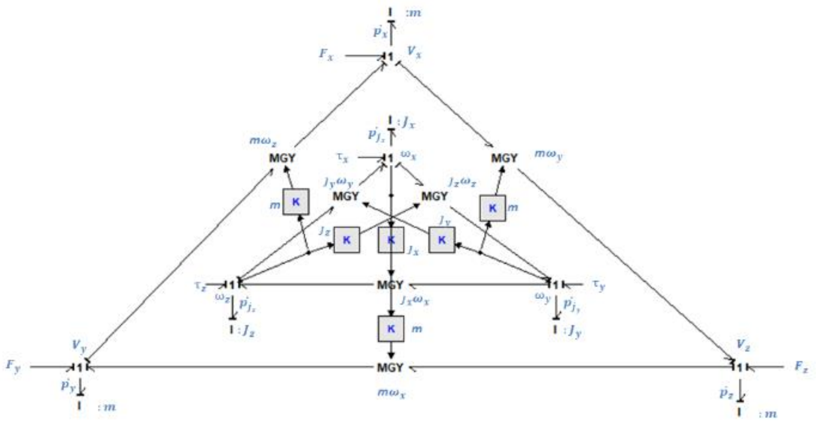

Figure 1. BGM of the main body of FUAV

3.5 Elastic wing model

In this section, we approximate the dynamic characteristics of the wing as an elastic beam in transverse vibration, pivoted at one end. In the proposed model, we measure mass and elasticity as distributed parameters. The two methods generally used for modeling a distributed system are finite lumping, and modal analysis. For the finite lumping method, a great number of reticulations are a must for accurate low frequency response. However, this increase in the reticulations yields inaccuracies at higher frequencies, as well as increases the number of states. Hence we use the modal approach to generate the bond graph model of our system, which is more accurate and flexible enough to be combined in the overall system model. The implementation of boundary conditions is also easy in the modular approach (Pourtakdoust & Aliabadi, 2012).

The modal approach, while being accurate, necessitates that the transformer for modal contributions be formed separately for several boundary conditions. Due to this, extension to the overall system model is not so simple. We integrate structural damping, which is normally small, by adding *R* elements to the 1-junctions showing motions of lumped or modal masses. Further, we attain the damping of rotational motions in the Euler-Bernoulli model by attaching a *C*-1-*R* module to the 0-junctions in which *C* elements signify flexural stiffness (Pourtakdoust & Aliabadi, 2012).

Furthermore, we model the flapping wing using Euler-Bernoulli beam as flexible element having pinned-free boundary conditions. Using Euler-Bernoulli beam, natural frequencies along with their modes used in the simulation can be analytically found. Moreover, the elastic flapping wing equation of motion using the Euler-Bernoulli elastic beam is to be integrated with aerodynamics and mass-inertia loadings. Consequently, this beam can be used as a good model alternative for a real elastic wing (Pourtakdoust & Aliabadi, 2012). Figure 5(a) illustrates the rigid and Euler-Bernoulli flexible beam subject to an external gust force *F* with respect to the hinge point.

The equation of motion of the elastic wing under transverse vibration due to external force is as follows (Jahanbin et al., 2016):

$$\mathrm{EI}\frac{\partial^4 w}{\partial x^4} + \rho A\,\frac{\partial^2 w}{\partial t^4} = \mathrm{F}\,\delta(\mathrm{x} - x_1) \qquad (9)$$

where EI, ρ, *A* and *w* are flexural rigidity, material density, cross-sectional area and deflection of the wing, respectively. The bending moments corresponding to the pivoted end are zero. Likewise, the shear force and bending moment associated to the free end are also zero. The mode shapes and frequency equation for pinned-free boundary conditions can be described as follows (Pourtakdoust & Aliabadi, 2012):

$$\tanh\beta_n l - tan\beta_n l = 0 \qquad (10)$$

$$Y_n(x) = (sin\boldsymbol{h}\beta_n l + sin\beta_n l)(cos\boldsymbol{h}\beta_n x + cos\beta_n x) - (cos\boldsymbol{h}\beta_n l + cos\beta_n l)(sin\boldsymbol{h}\beta_n x + sin\beta_n x) \qquad (11)$$

and $\beta_n l$ can be described as:

$$\beta_1 l = 3.92, \beta_2 l = 7.06, \beta_3 l = 10.2,\ \beta_4 l = 13.35, \beta l = 0 \text{ for rigid body} \qquad (12)$$

where the β_n represent the modal stiffness. Figure 5(b) shows the valid bond graph model of the elastic wing with one rigid mode and multiple flexible modes taken from (Jahanbin *et al.*, 2016). This bond graph is obtained from modal Equation (11) for *n* = 1, 2, 3, **…** The external force *F* (gust) stimulates each mode in accordance with Equation (9). The transformers shown are simply the mode shapes from Equation (11). Pinned-free boundary conditions resulted in one rigid mode and *n* elastic modes and are displayed in the bond graph. It is evident that the transformer elements attached to the rigid body mode apply the moment to these elements (Jahanbin *et al.*, 2016).

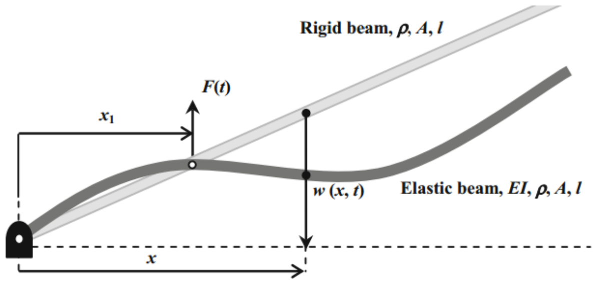

(a) Sketch of FUAV's elastic wing under transverse force F

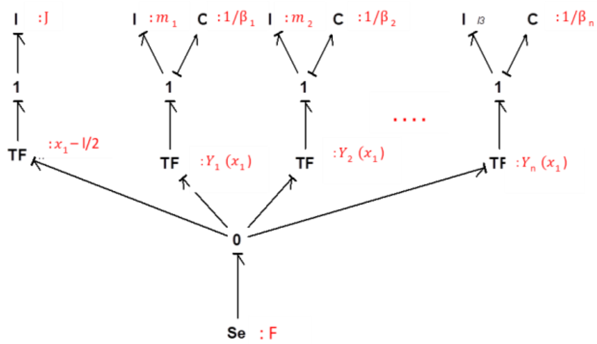

(b) BGM of a FUAV's elastic wing

Figure 5. Euler-Bernoulli Elastic Wing of FUAV (a) Sketch (b) BGM

3.6 BGM of gust mitigation system (GMS)

Development of BGM of GMS starting from a single electromechanical (EM) covert feather is presented in this section. For detailed formulation of the BGM of GMS, readers can refer to the author's previous work (Abbasi & Mahmood, 2019a, Abbasi & Mahmood, 2019b). The overall order of the BGM of EM feather is eight, since there are eight energy storing elements. There is the one disturbance input Sf (source of flow), which depicts a gust incident on the feather; and there are the two controllable inputs MSf (modulated source of flow) and MSe (modulated source of effort). These inputs form part of the input vector $\vec{u}(t)$. MSe is actually the force applied on the linkage, whereas MSf is the current input to the voice coil actuator.

The state variables consist of generalized momenta p_1, p_2, p_3 at every inertia element and generalized displacements q_1, q_2, q_3, q_4 at every compliance element. State variable q_5 is the state of displacement sensor used in the bond graph. The BGM obtained is used to formulate the state space equations (13)-(20). Figure 6 shows the BGM of GMS comprising 16 EM covert feathers.

$$\dot{p}_1 = ic \cdot p_3 + ic \cdot q_3 \tag{13}$$

$$\dot{q}_1 = \frac{1}{I_1} \cdot p_2 \tag{14}$$

$$\dot{p}_2 = \frac{ic}{l} p_3 + \frac{ic}{l} q_3 - \frac{1}{C} q_1 - \frac{1}{C_1} q_2 - \frac{m}{C_2} q_4 \tag{15}$$

$$\dot{q}_2 = \frac{1}{I_1} \cdot p_2 \tag{16}$$

$$\dot{p}_3 = q_5 \tag{17}$$

$$\dot{q}_3 = S_f - \frac{1}{l \cdot I_1} p_2 - \frac{1}{I} p_1 \tag{18}$$

$$\dot{q}_4 = \frac{m}{I_1} p_2 - \frac{R}{C_2} q_4 \tag{19}$$

$$\dot{q}_5 = \frac{1}{l \cdot I_1} p_2 \tag{20}$$

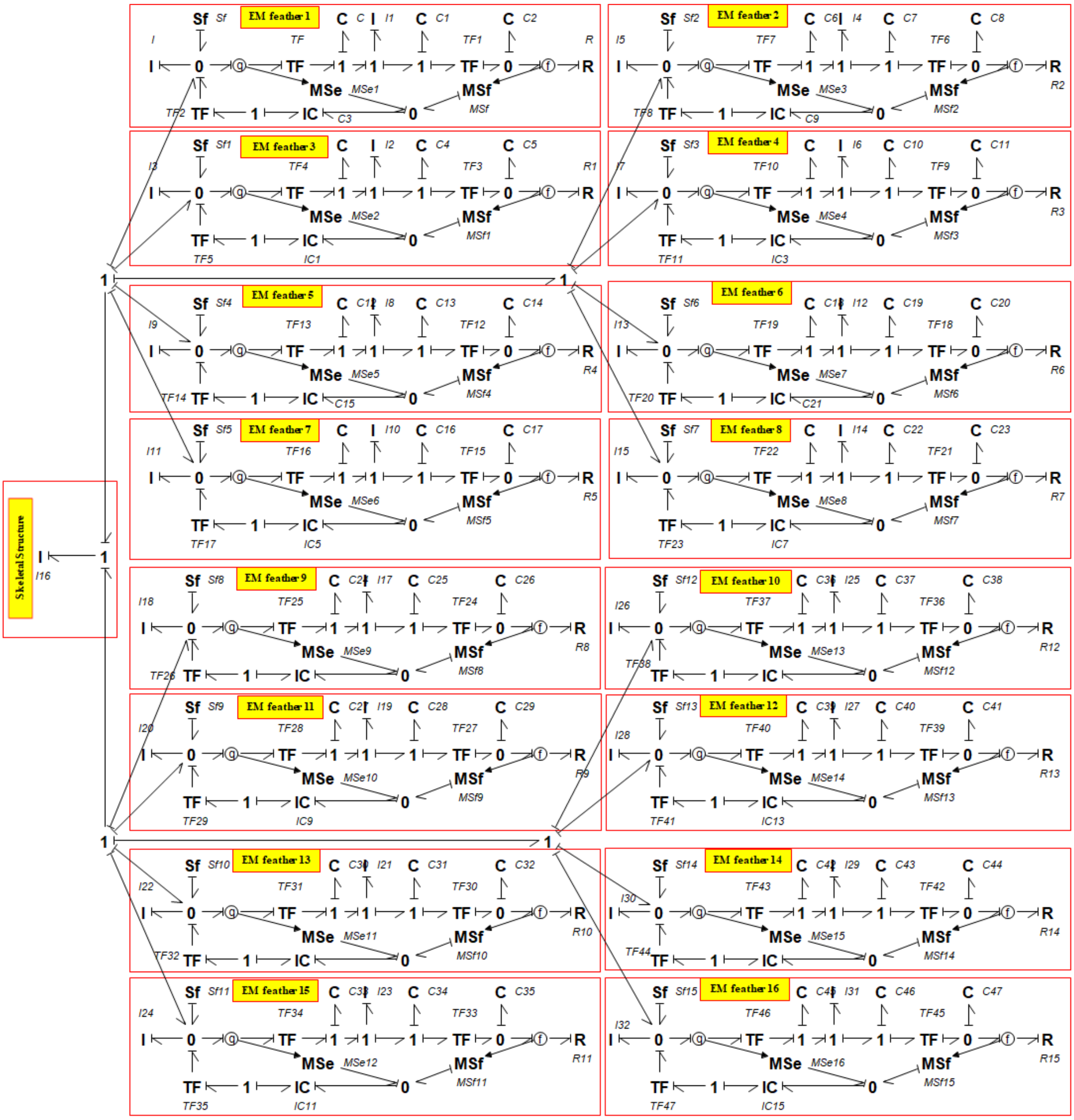

Figure 6. BGM of 16 EM feathers GMS

3.7 BGM of a complete gust mitigating FUAV

The BGM of the complete gust mitigating FUAV comprising the main body and the GMS incorporated flexible wings, driven by two DC motors and slider crank flapping mechanism, is presented in this section. The complete BGM of the Gust Mitigating FUAV is developed by joining the BGMs of the subsystems presented in previous sections using appropriate junctions, and is illustrated in Figure 7. It is important to mention here that the complete BGM of gust mitigating FUAV has been reduced to 8 EM covert feathers per wing to avoid modeling complexity, since a complete FUAV model comprising 16 feathers per wing results in 260th order model and is challenging to simulate. Moreover, this reduced model presents a baseline and is sufficient to prove efficacy of the proposed GMS design.

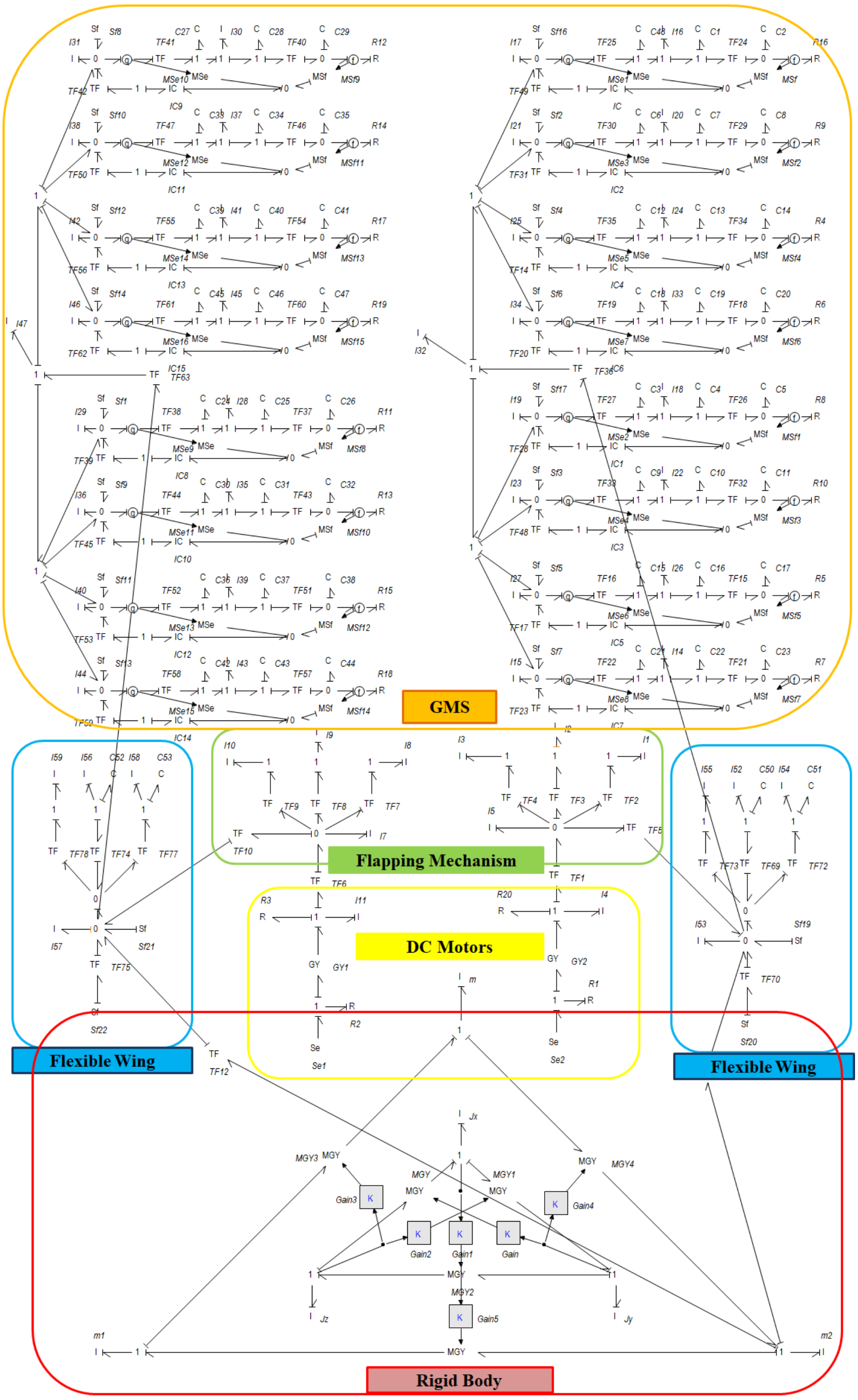

Figure 7. BGM of a complete gust mitigating flexible FUAV

State space of gust mitigating FUAV is derived from the BGM, as illustrated in Figure 7 using 20-SIM. The state matrix $\vec{x}(t)$ contains generalized momenta of inertia elements and generalized displacements of compliance elements. There are 18 disturbance inputs depicting gusts, which are applied to each EM covert feather. Additionally, the gust is applied to flexible wings as well as a source of flow i.e. *Sf* at 0 junction, and this also forms part of the disturbance input vector. There are 34 controllable inputs including; 2 sources of effort (S_e) representing the DC motors, 16 are displayed as modulated flow sources i.e. MS_f, and 16 are presented as modulated effort source i.e. MS_e. These 34 controllable inputs form parts of the input vector $\vec{u}(t)$. The final state matrix A comes out to be of size *146*x*146*, input gain matrix B comes out to be of size *146*x*34,* and the output gain matrix C comes out to be of size 34x146.

In this study the scope was only to simulate a vertical gust, which produces a lift force on the FUAV. The comprehensive modeling of a gust mitigating FUAV by integrating all aerodynamic and structural elements is complicated. For simplification certain assumptions are made that include neglecting a wide range of aerodynamic forces encountered by FUAV, which have been explored in a recent study (Chin & Lentink, 2016) i.e. thrust, drag, wing's wake, rotational inertia, circular rotation, rotational lift, leading edge vortex, viscous friction, and added mass. Addition of several boundary conditions, various input forces and moments, extra degrees of freedom, and moreover altering the wing's vibrational modes need to be further explored.

4. Results and Discussion

In order to ascertain the correctness of BGM of gust mitigating flexible FUAV developed in the above section we simulated three vertical gust speeds (35m/s, 25m/s, 15m/s) for effects on three feathers (feather no 1, feather no 2, and feather no 3) on the right wing of FUAV. Figure 8 depicts the responses of these 3 EM feathers at different gust speeds. The resultant forces on EM feathers produced through local controller are 0.51N, 0.33N & 0.16N, and the corresponding rotational velocities of the feathers are 22m/s, 18m/s and 14.5m/s, respectively. These figures evidently indicate that the peak values of forces and deflection speed of gust mitigating FUAV are in the correct ranges. It is also seen that the force and the corresponding speed of flaps are directly proportional to the gust force applied.

In order to prove efficacy of proposed design, two simulation scenarios are considered. First the flexible FUAV without GMS is simulated by applying 25m/s and 20 m/s gusts on its wing and the movement in z-direction is observed. Second, these two gusts are applied on the flexible FUAV with GMS installed as illustrated in Figure 7 and the corresponding motion in z-direction is analyzed. The simulations are performed for both the rigid wing and the flexible wing arrangements. The displacements in z-direction for all of these simulation scenarios are illustrated in Figure 9.

It can be clearly seen that the rigid wing gust mitigating FUAV has successfully alleviated the gust effect to 32%, while the flexible wing gust mitigating FUAV has successfully mitigated the gust to 34.9% because of the actuation of EM covert feathers installed on the wing as expected. These results confirm the anticipated utility of the

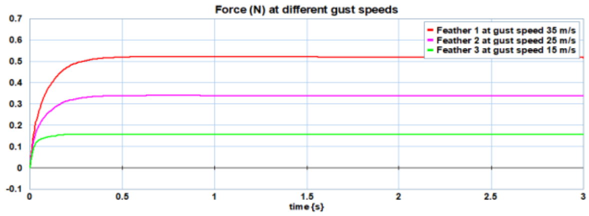

(a) Force on EM feathers

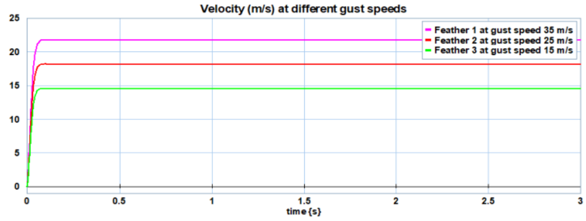

(b) Speed of EM feathers

Figure 8. Response of EM feathers at different gust speeds

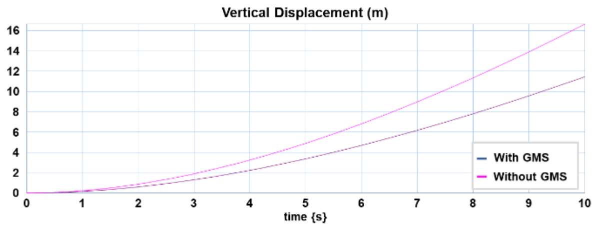

(a) FUAV with Rigid Beam Wing at 25 m/s gust

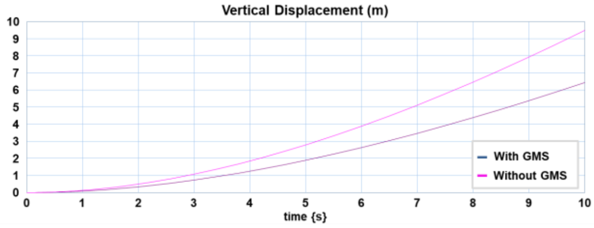

(b) FUAV with Rigid Beam Wing at 20 m/s gust

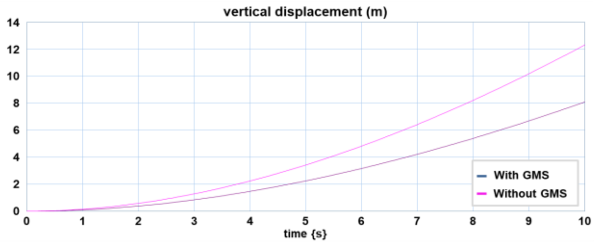

(c) FUAV with flexible Euler Bernoulli Beam Wing at 25 m/s gust

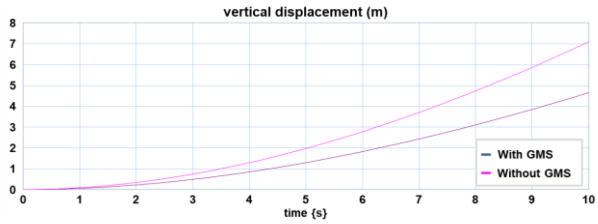

(c) FUAV with flexible Euler Bernoulli Beam Wing at 20 m/s gust

Figure 9. Displacement of FUAV in vertical direction at different gust speeds

proposed gust mitigating FUAV design and furthermore prove that the gust mitigating potential of flexible wings is superior to that of rigid wings. These simulation results are summarized in Table 1.

Figure 10 (a) shows a comparison of forward velocities of FUAV for different values of flexural rigidities of wings. It can be seen that the decrease in rigidity helps attain better aerodynamic performance and increased forward velocity. Moreover the forward velocities of the rigid wing FUAV in present research and in the study by (Karimian & Jahanbin, 2019) show close agreement. In addition, results attained in the current study are compared to the findings of experimental research by (Karimian & Jahanbin, 2019) and are summarized in Table 2. Very close agreement among the results of FUAV with GMS and FUAV without GMS, that are acquired in current work and experimental findings endorses accuracy and validity of the proposed design. Figure 10(b) depicts the comparison of roll angle of FUAV for different flexural rigidities of the wings. It can be seen that the decrease in rigidity reduces the roll angle and thus helps attain better aerodynamic performance due to increased stability.

Linearizing the model by taking gust speed on right wing (*Sf*) as input and force acting on wing (I_6) as output in 20-SIM software generates a 146th order model. The pole-zero plot of the flexible gust mitigating FUAV in Figure 11 shows multiple poles at origin and a few poles in the right half plane (RHP), so the system is internally unstable. The values of elements of BGM of gust mitigating FUAV presented in Figure 7 are shown in Table 3. It must be noted that elements of all 16 EM feathers are same as one EM feather and are taken from the author's previous work (Abbasi & Mahmood, 2019b).

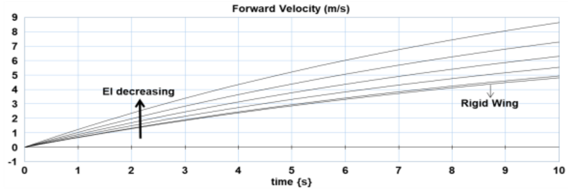

(a) Flexural Rigidity (EI) vs forward velocity

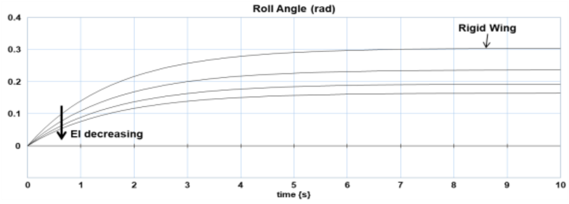

(b) Flexural Rigidity (EI) vs roll angle

Figure 10. Effect of Flexural Rigidity (EI) of wing on FUAV's aerodynamic performance

Table 2. Comparison between present work and experimental research

		Vertical displacement (m)
Current work	Without GMS	16.5
	With GMS	11.2
Experimental (Karimian & Jahanbin, 2019)		16.9

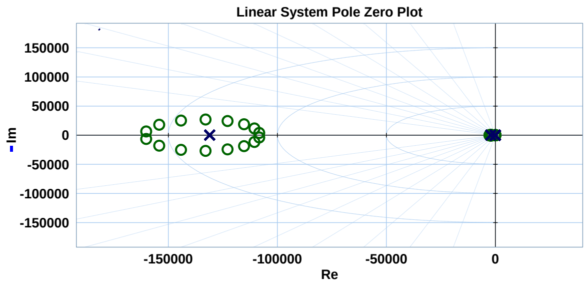

Figure 11. Open loop poles of the FUAV

5. Conclusions

We propose a design for a new Gust Mitigation System (GMS) for flapping wing UAV (FUAV) inspired by the covert feathers of birds. Addition of electromechanical (EM) covert feathers on the top and bottom wing surfaces of FUAV decreased the gusting forces exerted on an FUAV body. We developed a complete Bond Graph Model (BGM) of a FUAV containing the main rigid body, flapping system, GMS installed flexible wings, and the power system comprising battery, motor, and gearbox. The dynamic wing flexibility was modeled as an Euler-Bernoulli beam for realism. We used bond graph modeling for the development of a comprehensive model and performed simulations of the gust mitigating FUAV in 20-SIM software.

The simulation results show that wing flexibility enhances aerodynamic efficiency, and moreover the performance of proposed GMS for flexible wings is better than that with rigid wings during gusty airflows, since the flexibility increased forward velocity and reduced roll angle. In addition, it was also demonstrated that the gust mitigating potential of flexible wings is superior to that of rigid wings, since the rigid wing gust mitigating FUAV has alleviated the gust to 32% while the flexible wing gust mitigating FUAV has successfully mitigated the gust to 34.9%. The forward velocity of rigid wing FUAV in present research is 5m/s whereas that in experimental data is 4.8m/s. Also, the vertical displacement in present work is 16.5m and that in the literature is 16.9m. Strong agreement between experimental results and the present results validates the accuracy of proposed design and developed model. Furthermore, insight into model internal dynamics shows multiple poles at origin and a few poles in right half plan (RHP), indicating that the system is internally unstable and therefore merits the development of a controller.

Table 1. Vertical displacement of rigid and flexible FUAV at gust speeds 25 m/s & 20 m/s

Wing design	25 m/s gust			20 m/s gust		
	Without GMS	With GMS	Mitigation percentage	Without GMS	With GMS	Mitigation percentage
Rigid Wing FUAV	16.5 m	11.2 m	32 %	9.4 m	6.4 m	32 %
Flexible Wing FUAV	12.3 m	8 m	34.9 %	7.1 m	4.62 m	34.9 %

Table 3. Parameters of model

Component	Description	Value
Motors		
Voltage source	Electrical	7.2 V
Armature resistance of the motors	Electrical	5.1 Ω
Gyrator ratio of motors	Electrical	0.00813
Damping of motors	Mechanical	0.00068N-s/m
Mass of motors	Mechanical	0.021Kg
Gears		
Ratio of gears	Mechanical	0.112
Flapping Mechanism		
Mass moment of inertia of crank	Mechanical	0.009 Kg/m^2
Transformer ratio of connecting rod	Mechanical	2
Transformer ratio of linkages	Mechanical	1
Mass of connecting rod	Mechanical	0.03 Kg
Mass moment of inertia of connecting rod	Mechanical	0.006 Kg/m^2
Rigid Beam Wing		
Mass of rigid beam	Mechanical	0.4 Kg
Mass moment of inertia of rigid beam	Mechanical	0.024 Kg/m^2
Transformer ratio of rigid beam	Mechanical	1
Main Body		
Mass of body	Mechanical	0.15 Kg
Mass moment of inertia (J_x, J_y, J_z)	Mechanical	0.002,0.004,0.003 Kg/m^2
Gust speed	Mechanical	25 m/s
GMS		
Flap		
Mass of flap	Mechanical	0.018 kg
Mass of skeletal structure	Mechanical	0.098 kg
Gust velocity on feather	Mechanical	25 m/s
Voice Coil Actuator		
Inductance	Electrical	0.89 H
Stiffness	Mechanical	0.589 KN/m
Piezoelectric Stack		
Resistance between amplifier and PZT	Electrical	5 Ω
Mass of Stack	Mechanical	0.008Kg
PZT spring stiffness	Mechanical	0.024 kN/m
PZT equivalent capacitance	Electrical	$1.5x\ 10^{-7}$ F
Coupling Ratio	Electrical	0.478
Spring		
Spring stiffness	Mechanical	0.03kN/m
Mechanical Linkage		
Transformer Ratio	Mechanical	0.2

Since the present research is in its early stages, we made some assumptions to simplify the situation, such as ignoring aerodynamic forces encountered by FUAV including thrust, drag, wing's wake, rotational inertia, circular rotation, rotational lift, leading edge vortex, viscous friction and added mass. In the future, Computational Fluid Dynamics modeling of the presented design is planned. Furthermore, parametric dynamic study including sensitivity examination of the FUAV performance to several design parameters will be done. Moreover, various control schemes will be investigated for achieving stability of the gust mitigating FUAV.

Notation

GMS	Gust Mitigation System
BGM	Bond Graph Model
FUAV	Flapping Wing UAV
GAS	Gust Alleviation System
PZT	Piezoelectric transducer
EM	Electromechanical
UAV	Unmanned aerial vehicle
UAS	Unmanned aircraft system
CFD	Computational fluid dynamics
Sf	Source of flow
Se	Source of effort
MSf	Modulated source of flow
MSe	Modulated source of effort
TF	Transformer
GY	Gyrator
SJA	Synthetic jet actuators

References

Abbasi, S. H., & Mahmood, A. (2019a). Bio-inspired gust mitigation system for a flapping wing UAV: modeling and simulation. *Journal of the Brazilian Society of Mechanical Sciences and Engineering, 41*(11). doi:10.1007/s40430-019-2044-9

Abbasi, S. H., & Mahmood, A. (2019b). Modeling, simulation and control of a bio-inspired electromechanical feather for gust mitigation in flapping wing UAV. *2nd International Conference on Communication,* *Computing and Digital Systems (C-CODE)*, 195-200. doi:10.1109/C-CODE.2019.8681016

Blower, C. J., & Wickenheiser, A. M. (2011). The development of a closed-loop flight controller for localized flow control and gust alleviation using biomimetic feathers on aircraft wings. *Proceedings of the ASME Conference on Smart Materials, Adaptive Structures and Intelligent Systems 5109*, 699-705, doi:10. 1115/SMASIS2011-5109

Chin, D. D., & Lentink, D. (2016). Flapping wing aerodynamics: from insects to vertebrates. *Journal of Experimental Biology, 219*(7). 920-932. doi:10. 1242/jeb.042317

Fritz, T., & Long, L. (2004). Object-oriented unsteady vortex lattice method for flapping flight. *Journal of Aircraft, 41*(6), 1275–1290. doi:10.2514/1.7357

Jahanbin, Z., Ghafari, A. S., Ebrahimi, A., & Meghdari, A. (2016). Multibody simulation of a flapping-wing robot using an efficient dynamical model. *Journal of Brazilian Society of Mechanical Sciences and Engineering, 38*(1), 133–149. doi:10.1007/s40430-015-0350-4

Karimian, S., & Jahanbin, Z. (2019). Aerodynamic modeling of a flexible flapping-wing micro-air vehicle in the bond graph environment with the aim of assessing the lateral control power. *Proceedings of the Institution of Mechanical Engineers, Part G: Journal of Aerospace Engineering 233*(13), 4998–5015. doi: 10.1177/0954410019835980

Mohamed, A., Massey, K., Watkins, S., & Clothier, R. (2014). The attitude control of fixed-wing MAVS in turbulent environments. *Progress in Aerospace Sciences, 66*, 37-48. doi:10.1016/J.PAEROSCI. 2013.12.003

Pourtakdoust, S. H., & Aliabadi, S. K. (2012). Evaluation of flapping wing propulsion based on a new experimentally validated aeroelastic model. *Scientia Iranica, 19*(3), 472–482. doi:10.1016/J.SCIENT. 2012.03.004

Ratti, J., Moon, J., & Vachtsevanos, G.J. (2011). Towards low-power, low-profile avionics architecture and control for micro aerial vehicles. *2011 Aerospace Conference*, 1-8.

Send, W. (1992). The mean power of forces and moments in unsteady aerodynamics. *Zamm-zeitschrift Fur Angewandte Mathematik Und Mechanik, 72*, 113-132.

Tian, P., Chao, H., Rhudy, M. B., Gross, J. N., & Wu, H. (2021). Wind sensing and estimation using small fixed-wing unmanned aerial vehicles: A survey. *Journal of Aerospace Information Systems, 18*, 132-143. doi:10.2514/1.I010885